Available online at www.sciencedirect.com
ScienceDirect
Pattern Recognition 40 (2007) 2861–2873
PATTERN RECOGNITION
THE JOURNAL OF THE PATTERN RECOGNITION SOCIETY
www.elsevier.com/locate/pr

Semi-automatic computer aided lesion detection in dental X-rays using variational level set

Shuo Li[a,*], Thomas Fevens[b], Adam Krzyżak[b], Chao Jin[b], Song Li[c]

[a]*GE Healthcare, London, Canada*
[b]*Medical Imaging Group, Department of Software Engineering and Computer Science, Concordia University, Montréal, Que., Canada*
[c]*School of Stomatology, Anhui Medical University, Hefei, Anhui, PR China*

Received 23 January 2006; received in revised form 14 November 2006; accepted 3 January 2007

Abstract

A semi-automatic lesion detection framework is proposed to detect areas of lesions from periapical dental X-rays using level set method. In this framework, first, a new proposed competitive coupled level set method is used to segment the image into three pathologically meaningful regions using two coupled level set functions. Tailored for the dental clinical setting, a two-stage clinical segmentation acceleration scheme is used. The method uses a trained support vector machine (SVM) classifier to provide an initial contour for two coupled level sets. Then, based on the segmentation results, an analysis scheme is applied. Firstly, the scheme builds an uncertainty map from which those areas with radiolucent will be automatically emphasized by a proposed color emphasis scheme. Those radiolucent in the teeth or jaw usually suggested possible lesions. Secondly, the scheme employs a method based on the average intensity profile to isolate the teeth and locate two types of lesions: periapical lesion (PL) and bifurcation lesion (BL). Experimental results show that our proposed segmentation method is able to segment the image into pathological meaningful regions for further analysis; our proposed framework is able to automatically provide direct visual cues for the lesion detection; and when given the orientation of the teeth, it is able to automatically locate the PL and BL with a seriousness level marked for further dental diagnosis. When used in the clinical setting, the framework enables dentist to improve interpretation and to focus their attention on critical areas.

Keywords: Dental X-rays; Level set; Image segmentation; Support vector machine; Detection; Machine learning; Principal component analysis

1. Introduction

The diagnosis of many dental anomalies would be impossible without radiographs, because of their location in the mineralized tissues (bone and teeth) or because they are hidden under the surface of the cortical plate that cannot be seen during a visual examination in dental practices. The use of radiographs is indispensable during the treatment phase, e.g., during root canal treatment to monitor the progress of the root preparation, or to know the orientation of wisdom molars to be extracted. The effect of dental treatment of bony structures, e.g., the treatment of periodontal defects or the success of an apicoectomy, can be established by radiographic examination only. The past few years has seen a great increase in the usage of digital dental X-rays. Advantages of digital dental X-rays are the immediate availability of the images, the lower radiation dose, the possibility of image enhancement, image reconstruction. And more importantly, digital dental X-rays make computer aided dental X-rays analysis possible and convenience.

Besides being used for clinical purposes, dental X-rays are also widely used in forensic identification. Jain et al. [1–4] are developing an automatic human identification system using dental X-rays.

However, although digital dental X-rays are becoming widely used, it is a challenging task to do automatic, or even semi-automatic, computer aided dental X-rays analysis. As shown in Fig. 1, as compared with other types of images, dental X-rays analysis is a challenging problem for classic image processing methods due to the following characteristics: (1) poor image

* Corresponding author. Tel.: +1 519 317 8922.
E-mail addresses: shuo.li@ge.com (S. Li), fevens@cs.concordia.ca (T. Fevens), krzyzak@cs.concordia.ca (A. Krzyżak), chao_jin@cs.concordia.ca (C. Jin), xlisong@sohu.com (S. Li).

0031-3203/$30.00
doi:10.1016/j.patcog.2007.01.012

modalities: noise, low contrast, and sampling artifacts; (2) complicated topology; (3) arbitrary teeth orientation; and (4) lack of clear lines of demarcation between regions of interest, which is especially true for dental X-rays since problem teeth tend to have very complicated structures and are normally coupled with healthy teeth. Therefore dental X-rays are normally inspected by a dentist. Although efficient, human inspection requires specialized training and a dentist's time, which are increasingly expensive. Moreover, human inspection gives a subjective judgment, which may vary from dentist to dentist, and, as such, does not give a quantitative measurement. Inspection results could be affected by many factors, such as fatigue and distraction by other features, especially the main features they are looking for, in the image, for example. Also, some early lesions may not be even visible to the human eye. All of these issues indicate a need for effective automatic or semi-automatic dental X-rays analysis.

In this paper, we report on an innovative work, which explores the possibility of semi-automatically providing indications and visual cues to the dentist to aid in determining areas of lesion especially those lesions below the cortical plate. Moreover, two particular lesions will automatically locate periapical lesion (PL) and bifurcation lesion (BL), which are the primary reasons that X-rays are taken in many countries, once the orientation of the teeth is manually given. Early detection of those lesions is very important since often they can be remedied by dental procedures. Without early treatment, they might lead to tooth loss or resorption of the alveolar bone. Although the approach developed here can be applied to other types of dental X-rays, we will be dealing primarily with periapical X-rays, which are close-up views of a few individual teeth including the root and surrounding bone. Periapical X-rays is very useful in diagnosing an abscess, impacted tooth or bone loss due to periodontal disease. Compared with panoramic dental X-rays, which is the tomography of the entire jaw region, periapical X-rays taken for these purposes are more challenging since the orientation of the teeth may not be fixed and problem areas are either complicated, as shown in Fig. 1(a), or easily overlooked, as shown in the circled areas in Fig. 1(b) and (c). These factors complicate the use of traditional image processing methods. Therefore, we employ one of the modern techniques from image processing, referred as the level set method [5]. The application of the level set method in medical image segmentation is popular due to its ability to capture the topology of shapes in medical imagery and its robustness to noise. A level set segmentation method is proposed for dental X-ray images. In our previous work [6,7], we proposed a level set segmentation method for dental X-ray image. The segmentation method employs three coupled level sets driven by a proposed pathologically variational modeling. The benefit of using level set segmentation on dental X-rays will be discussed in detail in Section 2.2.

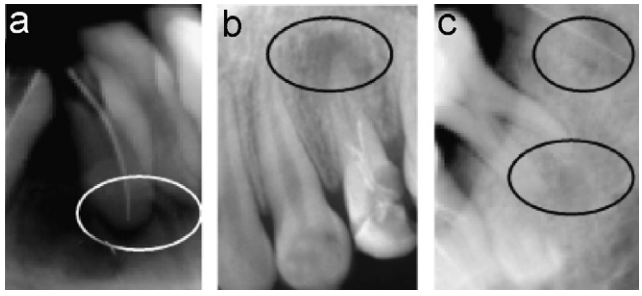

Fig. 1. Dental X-rays examples.

To analyze dental X-rays to determine area of lesions, a semi-automatic computer aided dental X-rays analysis framework is proposed. The framework consists of two phases: segmentation and analysis. Segmentation contains two stages: training and clinical segmentation. The diagram of the proposed framework is shown in Fig. 2. Analysis phase contains three steps: uncertainty map building, lesion detection and location of PL and BL. To the best of our knowledge, we are the first group working towards automatic computer aided dental X-ray diagnosis for the detection of lesions in dental X-ray using the level set method. This paper reports on our preliminary results towards this goal.

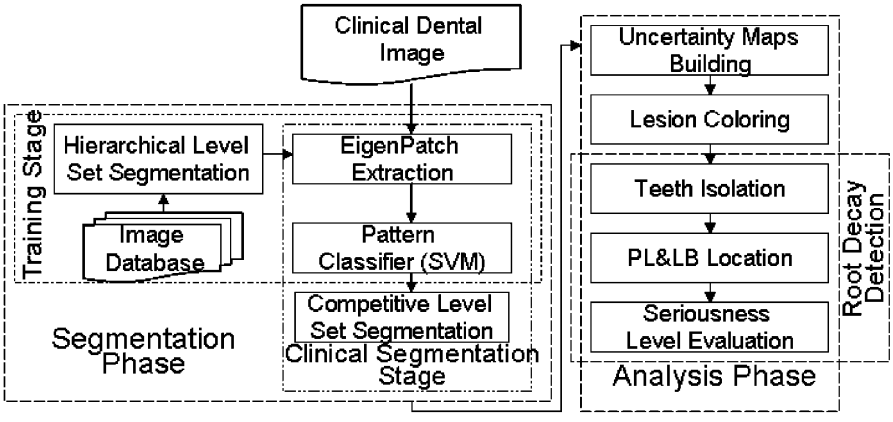

Fig. 2. Framework diagram.

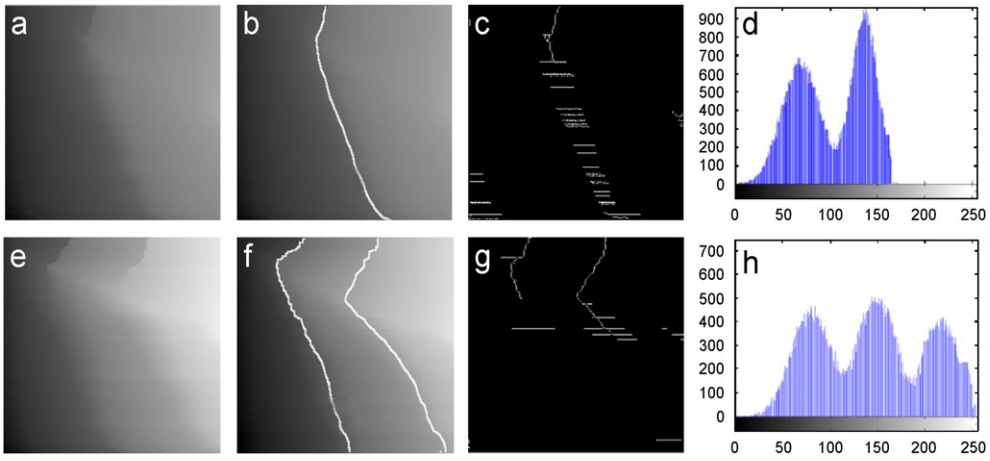

Fig. 3. (a) Original image. (b) Variational level set segmentation by Chan and Vese [15]. (c) Results by Sobel Edge detection. (d) Histogram image of (a). (e) Original image. (f) Variational level set segmentation by Samson et al. [19]. (g) Results by Sobel Edge detection. (h) Histogram image of (e).

2. Variational level set and dental X-rays

2.1. Level set method

Proposed by Osher and Sethian [5], level set methods have attracted more and more attentions from researchers in different areas [8–10]. In problems of curve evolution, the level set method has been used extensively, because it allows for image characteristics such as curps, corners, and automatic topological changes. Moreover, the discretization of the problem is made on the fixed rectangular grid.

Let Ω be a bounded open subset of R^2, with $\partial\Omega$ as its boundary. Let $U_0 : \Omega \to R$ be a given image, and $C : [0, 1] \to R^2$ be a parameterized curve. The curve C is represented implicitly via a Lipschitz function ϕ by $C = \{(x, y)|\phi(x, y) = 0\}$, and the evolution of the curve is given by the zero-level curve at time t as the function $\phi(t, x, y)$. To solve the differential equation, the curve C is evolved in the normal direction with speed F.

$$\begin{cases} \dfrac{\partial\phi}{\partial t} = |\nabla\phi|F, \\ \phi(0, x, y) = \phi_0(x, y), \end{cases} \tag{1}$$

where the set $C = \{(x, y)|\phi_0(x, y) = 0\}$ defines the initial contour. A particular case is the motion by mean curvature, when $F = div(\nabla\phi/|\nabla\phi|)$ is the curvature. The equation becomes

$$\begin{cases} \dfrac{\partial\phi}{\partial t} = |\nabla\phi|\, div\left(\dfrac{\nabla\phi}{|\nabla\phi|}\right), \\ \phi(0, x, y) = \phi_0(x, y), \end{cases} \tag{2}$$

where ϕ_0 is initial level set function.

2.2. Variational level set segmentation

The level set method has become increasingly common in image processing due to its ability to capture the topology of shapes in medical imagery. We refer the reader to the review articles [11–13] for more details. The variational level set method, which derives the level set function by energy minimization, was first proposed by Zhao et al. [14] and is now a very popular approach for image segmentation [15–22]. Due to the energy minimization, the variational level set method naturally segments the image according to the energy functional. Due to this characteristic, as shown in Fig. 3, a variational level set method is able to detect a boundary where traditional methods fail. Moreover, the variational level set method is very robust to noise, which presents serious challenge to many traditional image processing techniques on dental X-rays, such as segmentation and feature detection. A detailed description of the advantages of using variational level set for dental X-rays in terms of noise robustness can be found in Refs. [6,7].

In the following, different related variational level set methods are reviewed.

Zhao et al. [14] proposed a coupled level set method for the motion of multiple junctions (e.g., of solid, liquid, and grain boundaries). They use an energy functional consisting of surface tension (proportional to length) and bulk energies (proportional to area) as shown in Eq. (3). This approach combines the level set method with a theoretical variational formulation. Assume there are n disjoint regions $\Omega_i (1 \leqslant i \leqslant n)$ in the image. The common boundary between Ω_i and Ω_j is denoted as $\Gamma_i j$. Zhao et al.'s functional can be expressed as

$$\begin{aligned} inf\, E = & \sum_{1 \leqslant i \leqslant j \leqslant n} f_{ij}\, Length(\Gamma_{ij}) + \sum_{1 \leqslant i \leqslant n} v_i \\ & \times Area(inside(C_i)). \end{aligned} \tag{3}$$

The level set function they obtain is expressed as

$$\begin{cases} \dfrac{\partial\phi_i}{\partial t} = |\nabla\phi_i|\left(\gamma_i\, div\left(\dfrac{\nabla\phi}{|\nabla\phi|}\right) - e_i - \lambda\left(\sum_{j=1}^{n} H(\phi_j) - 1\right)\right), \\ \dfrac{\partial\phi_i}{\partial \boldsymbol{n}} = 0 \quad \text{on } \partial\Omega, \end{cases} \tag{4}$$

where $\boldsymbol{n}$ denotes the exterior to the boundary $\partial\Omega$, and $\partial\phi/\partial\boldsymbol{n}$ denotes normal derivative of ϕ at the boundary.

Chan et al. [15,18] proposed a Mumford–Shah functional for level set segmentation. They add a minimal variance term E_{MV}. This model is able to detect contours both with or without a gradient. Objects with smooth boundaries or even with discontinuous boundaries can be successfully detected. Moreover, they claim this model is robust to the position of the initial contour. The 2D version of the model can be expressed as

$$inf_{(c_1,c_2,C)} E = \mu\, Length(C) + v\, Area(Inside(C)) + E_{MV},$$

with

$$E_{MV} = \lambda_1 \int_{inside(C)} (u_0(x,y) - c_1)^2 \,dx\,dy + \lambda_2 \int_{outside(C)} (u_0(x,y) - c_2)^2 \,dx\,dy,$$

where c_i are the averages of u_0 inside and outside C, and $\mu \geqslant 0$, $v \geqslant 0$, $\lambda_1 > 0$ and $\lambda_2 > 0$ are fixed parameters.

The level set function they obtain is given by

$$\begin{cases} \dfrac{\partial \phi}{\partial t} = \delta_\varepsilon(\phi)\left[\mu \cdot div\left(\dfrac{\nabla \phi}{|\nabla \phi|}\right) - v - \lambda_1(u_0 - c_1)^2 + \lambda_2(u_0 - c_2)^2\right] = 0, \\ \phi(0,x,y) = \phi_0(x,y) \quad \text{in } \Omega, \\ \dfrac{\delta_\varepsilon(\phi)\partial\phi}{|\nabla\phi|\partial \boldsymbol{n}} = 0 \quad \text{on } \partial\Omega, \end{cases}$$

where $\boldsymbol{n}$ denotes the exterior to the boundary $\partial\Omega$, $\partial\phi/\partial\boldsymbol{n}$ denotes the normal derivative of ϕ at the boundary and δ_ε is the Dirac delta function.

The Chan and Vese functional is very good for segmenting an image into two regions. To segment images with multiple regions we use Samson's method. In Ref. [19], Samson et al. presented a variational approach as shown in Eqs. (5) and (6).

$$inf\ E = \sum_{1 \leqslant i \leqslant j \leqslant n} f_{ij}\, Length(\Gamma_{ij}) + \sum_{1 \leqslant i \leqslant n} v_i\, Area(Inside(C_i)) + \sum_i \int_{\Omega_i} e_i \frac{(u_0 - c_i)^2}{\sigma_i^2} \,dx\,dy + \frac{\lambda}{2} \int \left(\sum_{j=1}^{n} H(\phi_j) - 1\right)^2 dx\,dy, \tag{5}$$

where Γ_{ij} is the intersection of different regions and σ_i is the variance. The level set function obtained is given by

$$\begin{cases} \dfrac{\partial \phi_i}{\partial t} = \delta_\varepsilon(\phi_i)\left(\gamma_i\, div\left(\dfrac{\nabla \phi}{|\nabla \phi|}\right) - e_i \dfrac{(u_0 - c_i)^2}{\sigma_i^2} - \lambda\left(\sum_{j=1}^{n} H(\phi_j) - 1\right)\right), \\ \dfrac{\partial \phi_i}{\partial \boldsymbol{n}} = 0 \quad \text{on } \partial\Omega, \end{cases} \tag{6}$$

where $H(\cdot)$ is the Heaviside function.

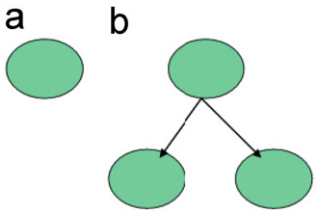

Fig. 4. Binary tree representation of hierarchical segmentation: first level segmentation by which, an image (a) is segmented into two regions by the one level set function as shown in (b).

To extend this two region segmentation method to multiple regions segmentation, hieratically scheme is usually employed [10,21,23]. Hierarchical level set segmentation employs an hierarchical approach to extend two region segmentation method to multiple regions segmentation. The idea is described by the binary trees in Figs. 4 and 5. The image is first segmented into two regions by one level set function as shown in Fig. 4. Then based on the variance analysis of each region, the program decides to further segment one (see Fig. 5(a) and (b)) or both regions (see Fig. 5(c)). The procedure is done recursively until the whole image is properly segmented. The advantage of the hierarchical level set is its easy implementation and fast segmentation. By the analysis of the region intensity variance, which measures the deviation from homogeneity of the regions, the hierarchical level set segmentation can easily be used as an automatic segmentation scheme using only one level set function.

3. Proposed framework

For the proposed framework, we first employ level set methods to segment the image into three regions: normal region (NR), potentially abnormal region (PAR), abnormal and background region (ABR). Designed for the dental clinical setting, the segmentation contains two stages: a training stage and a clinical segmentation stage. During the training stage, first, manually chosen representative images are segmented using hierarchical level set region detection. Then the results are used to train an SVM classifier. During the clinical segmentation stage, dental X-rays are first classified by the trained SVM, which provides initial contours for two coupled competitive level set functions. The competition of the two level set functions, as described in the next section, will give the final segmentation result. Based on the segmentation results, an analysis scheme is applied. The scheme first builds an uncertainty map, which is then used to automatically mark any areas of radiolucent since often those areas indicates bone loss, decay and etc. Subsequently, an average intensity profile-based method is employed to isolate the teeth and locate the two particular liaisons: PL and BL.

3.1. Competitive variational level set segmentation

In Refs. [6,7,24], Li et al. showed that variational level set can be modeled with a pathologically meaningful energy

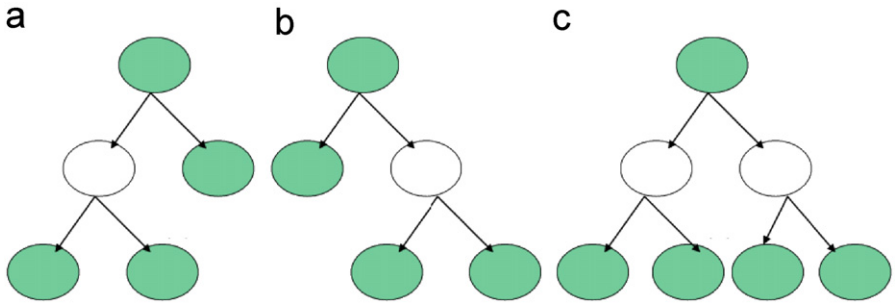

Fig. 5. Binary tree representation of hierarchical segmentation: second level segmentation by which, two segmented regions are further segmented into up to four regions. (a) and (b) show that only one of the two regions is further segmented into two regions. (c) shows that both regions are each further segmented into two regions.

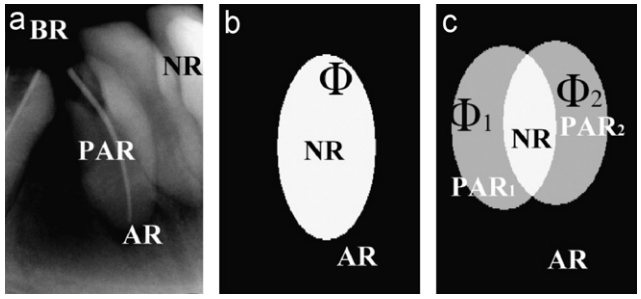

Fig. 6. Region modeling. (a) The dental X-ray image can be divided into four regions: Ω_{NR}, Ω_{PAR}, Ω_{AR}, and Ω_{BR}. (b) With one curve C, one level set function segments the image into Ω_{NR} and Ω_{AR}. (c) Two competitive coupled level set functions segment the image into three regions: Ω_{NR}, Ω_{PAR} and Ω_{ABR}.

function, which will automatically give a pathologically meaningful segmentation. In this implementation, we propose a new variational level set segmentation method driven by a new proposed pathological energy modeling. By the competition of two coupled level set functions, the segmentation segments the image into three pathological meaningful regions: NR, PAR, ABR. The modeling explicitly incorporates problem regions as part of the modeling, such that the identification of these areas would be an automatic product of the segmentation.

3.1.1. Pathological energy modeling

With an evolving curve C, one level set function divides the image (u) into two parts: Normal Region Ω_{NR}("+" region) and Abnormal Region Ω_{AR}("−" region) as shown in Fig. 6(b). The energy functional is given by

$$E(\Phi) = \beta_1 \int_{\Omega_{NR}} \frac{(u - c_{NR})^2}{\sigma_{NR}^2}\,\mathrm{d}x\,\mathrm{d}y + \beta_2 \int_{\Omega_{AR}} \frac{(u - c_{AR})^2}{\sigma_{AR}^2}\,\mathrm{d}x\,\mathrm{d}y, \tag{7}$$

where c_i is the mean grey value of the region Ω_i, σ_i is the variance and β_i is a constant.

However, for medical diagnosis and early detection, the areas between the NR and AR are more important since these are the areas of potential problems, which are of particular interest for medical diagnosis and early detection of problems. Therefore, we propose a competitive level set model with two level set functions to segment the image into three regions: NR, AR and PAR. As shown in Fig. 6(a), a dental X-ray image (u_0) can be divided into four regions of interest: the Normal Region (Ω_{NR}), the Potentially Abnormal Region (Ω_{PAR}); the Abnormal Region (Ω_{AR}) and the Background Region (Ω_{BR}). Since Ω_{AR} and Ω_{BR} is not separable in terms of intensity values, so in the segmentation, we take Ω_{AR} and Ω_{BR} to be a single region: the abnormal and background region (Ω_{ABR}). The energy functional for the two coupled level set functions (Φ_1 and Φ_2) can be modeled as

$$\begin{aligned} E(\Phi_1, \Phi_2) = {} & \lambda_1 \int_{\Omega_{NR}} \frac{(u - c_{NR})^2}{\sigma_{NR}^2}\,\mathrm{d}x\,\mathrm{d}y \\ & + \lambda_3 \int_{\Omega_{ABR}} \frac{(u - c_{ABR})^2}{\sigma_{ABR}^2}\,\mathrm{d}x\,\mathrm{d}y \\ & + \lambda_2 \int_{\Omega_{PAR}} \mathrm{Min}\left(\frac{(u-c_{PAR_1})^2}{\sigma_{PAR_1}^2}, \frac{(u-c_{PAR_2})^2}{\sigma_{PAR_2}^2}\right) \\ & \times \mathrm{d}x\,\mathrm{d}y, \end{aligned} \tag{8}$$

where the function $\mathrm{Min}(x, y)$ returns the smaller value of x and y, and λ_i is a constant. The modelling is in the same spirit as multiphase modeling in Ref. [18].

As shown in Fig. 6(c), using competitive coupled level set functions, if both level set functions classify an area as a normal region, we take it as a normal region Ω_{NR}; if both level set functions classify a region as an abnormal and background region, we take it as an abnormal and background region Ω_{ABR}; however, if only one of the level set functions segments a region as a NR, the region will be taken as a potentially abnormal region Ω_{PAR}. Using the proposed method, a segmentation can be naturally achieved by the competition of the two level set functions.

Although it is possible to use three coupled level set functions to segment the image into three regions as described in Refs. [6,7,24], the two coupled level set method is able to achieve

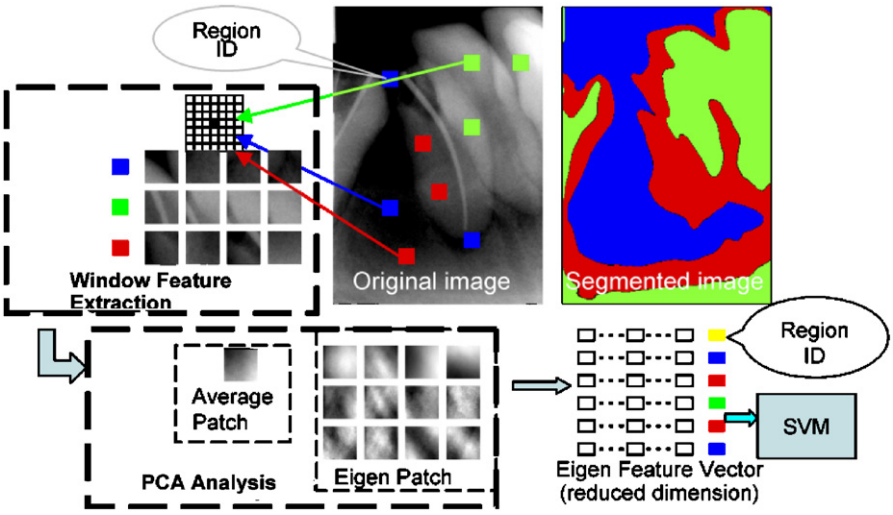

Fig. 7. Feature extraction diagram.

faster segmentation and a more accurate boundary as discussed in Refs. [18]. This is because two coupled level set method maintain one less level set function than three level sets method. Moreover, as described in Ref. [18], the vacuum ("−" areas of all level set functions) and overlap ("+" areas of all level set functions) of three level set function cost extra computational time and possible instability.

To achieve a fast and robust segmentation, a hybrid coupled level sets functional that combines minimal variance (Eq. (8)), the optimal edge integrator [20] and the geodesic active contour model [25] is used:

$$E = E(\Phi_1, \Phi_2) - \gamma_1 E_{LAP} + \gamma_2 E_{GAC}, \tag{9}$$

where γ_i are constants.

The geodesic active contour (E_{GAC}) and edge functional (E_{LAP}) are defined in Eq. (10).

$$E_{GAC}(C) = \int\int g(C)\,\mathrm{d}x\,\mathrm{d}y$$
$$E_{LAP}(C) = \int_C \langle \nabla, \mathbf{n}\rangle \mathrm{d}s + \int\int_{\Omega_C} K_u |\nabla_u|\,\mathrm{d}x\mathrm{d}y. \tag{10}$$

Here K_u is the mean curvature of the level set function, $\mathbf{n}$ is the unit vector normal to the curve and $\mathrm{d}s$ is the arc length of curve C. Function $g(x, y)$ is an inverse edge indicator function introduced in Ref. [25], and defined as $g(x, y) = \alpha^2/(\alpha^2 + |\nabla u|^2)$, where α is a constant and ∇ is the gradient operator.

The edge functional was proposed in Ref. [20] where the authors show that a Laplacian edge detector Δu provides optimal edge integration with regards to a very natural geometric functional. The detailed advantage and analysis of the geodesic active contour functional and Laplacian edge functional can be found in Refs. [20,25]. The similar hybrid function has been used in the hierarchical level set method [16] and the coupled level sets method [22].

3.1.2. Competitive level set functions

The level set function Φ_i are derived from the functional in Eq. (9) as shown in Eqs. (11) and (12).

$$\frac{\partial \Phi_1}{\partial t} = \delta_\varepsilon(\Phi_1)\left[\gamma_2\, div\left(g\frac{\nabla\Phi_1}{|\nabla\Phi_1|}\right) - \frac{(u-c_{NR})^2}{\sigma_{NR}^2}H(\Phi_2) - \frac{(u-c_{PAR})^2}{\sigma_{PAR}^2}(1-2H(\Phi_2)) + \frac{(u-c_{ABR})^2}{\sigma_{ABR}^2} \times (1-H(\Phi_2)) - \gamma_1 U_{\xi\xi}\right], \tag{11}$$

$$\frac{\partial \Phi_2}{\partial t} = \delta_\varepsilon(\Phi_2)\left[\gamma_2\, div\left(g\frac{\nabla\Phi_2}{|\nabla\Phi_2|}\right) - \frac{(u-c_{NR})^2}{\sigma_{NR}^2}H(\Phi_1) + \frac{2(u-c_{PAR})^2}{\sigma_{PAR}^2}H(\Phi_1) + \frac{(u-c_{ABR})^2}{\sigma_{ABR}^2} \times (1-H(\Phi_1)) - \gamma_1 u_{\xi\xi}\right]. \tag{12}$$

Here, $H(.)$ is the Heaviside function, $div(.)$ is the divergence operator, and $u_{\xi\xi} = \Delta u - Ku|\nabla u|$.

Although we only apply the proposed level set method to the dental X-rays, the method can be extended to be a general segmentation method. Three regions medical image segmentation plays an essential role in medical image processing since most X-rays and some types of CT images naturally contain up to three regions of interest.

3.2. Segmentation

As indicated in Ref. [22], although efficient, level set method is not suitable for clinical segmentation. This is not only because it is usually a time consuming method, when coupled with complicated medical structure, level set functions can be very time consuming, but also because that level set is sensitive to the placement of initial contour. Therefore, the running time

of level set method heavily relies on the position and size of the initial curves and the complexity of objects, coupled level set function do not converge for some initial curves and for some cases, different initial contours may given different segmented results. To achieve a fast and robust level set method in dental clinical setting, we adapt the clinical segmentation acceleration framework proposed by Li et al. [22]. Usually, numerical solution of the level set starts the initial contour as circle or ellipse, which is slow and not robust. The framework uses a support vector machine (SVM) classifier to provide initial contours closing to the final segmentation results for the level set functions, which greatly speeds up convergence of the coupled level set functions. Following the same principle, we use a SVM classifier to provide initial contours for two coupled level set functions. The purpose is not only to speed up the segmentation convergence as described in Ref. [22], but also to provide competitive initial conditions for the level set functions. The segmentation phase has two stages: a training stage and a clinical segmentation stage.

3.2.1. Training stage

During the training stage, manually chosen representative images are segmented by hierarchical level set region detection [10,21,23] using the Chan and Vese level set method [15] as described in Section 2.2. In hierarchical level set region detection, first a level set function is used to separate Ω_{ABR} from the rest of the image (Ω_{AR} and Ω_{BR}). Then another level set function is used to separate Ω_{AR} and Ω_{BR}. Then these results are used to train an SVM classifier. The SVM classifier we use is modified from Ref. [26]. A eigenpatch feature extraction is used to extract features for SVM. The procedure of the feature extraction is illustrated in Fig. 7. The feature we use is window-based feature vector, as shown in Fig. 7(a), processed by principal component analysis (PCA), as shown inFig. 7(b). With reference to eigenface [27,28], in this paper, the feature after PCA analysis is referred as an Eigenpatch. The PCA method here is adapted from the eigenface method [27,28].

The PCA analysis can be described as: let the features Γ_i ($i = 1, \ldots, M$) constitute the training set (Γ). The average matrix ($\overline{\Gamma}$) and covariance matrix C are

$$\begin{aligned}
&\overline{\Gamma} = \frac{1}{M}\sum_{i=1}^{M}\Gamma_i,\\
&\Phi_i = \Gamma_i - \overline{\Gamma},\\
&C = \frac{1}{M}\sum_{i=1}^{M}\Phi_i^{\mathrm{T}}\Phi_i = AA^{\mathrm{T}},\\
&L = A^{\mathrm{T}}A(L_{n,m} = \Phi_n^T\Phi_m),\\
&u_i = \sum_{k=1}^{M} v_{ik}\Phi_k(l = 1, \ldots, M),
\end{aligned} \tag{13}$$

where L is a $M \times M$ matrix, v_{ik} are the M eigenvectors of L and u_i are eigen-patches, which was called eigenfaces in Refs. [27,28]. The advantage of the PCA analysis here is its ability to remove the effects of noise and also to accelerate the classification by reduced feature dimension.

3.2.2. Clinical segmentation stage

During the clinical segmentation stage, the clinical dental X-ray image is first classified by the trained SVM. The classifier is able to give a rough classification of the three regions (Ω_{ABR}, Ω_{NR} and Ω_{PAR}), which may not be accurate. But it provides initial contours, closing to final segmentation results, for coupled level set functions as described in Refs. [21,22]. The final segmentation will be achieved by evolution of these two level set curves under the functional described in Eq. (9) and level set function described in Eqs. (11) and (12). The competitive initial conditions are set as following: for Φ_1, we set classified Ω_{NR} as the "+" region and rest of the image as the "−" region; for Φ_2, we set classified Ω_{NR} and Ω_{PAR} region as the "+" region and rest of the image as the "−" region.

3.3. Analysis phase

The analysis phase contains three steps: uncertainty map building, lesion coloring, and PL and BL detection. The first two steps are fully automatic. The only manual input for the last step is the image orientation. This information is not difficult to obtain in the dental clinical setting.

3.3.1. Uncertainty map

After the segmentation, for each image, an uncertainty map is built based on the following uncertainty measurement:

$$\psi = \frac{(u - c_{NR})\tau_1 + (u - c_{PAR})(\tau_2 - 2\tau_1) + (u - c_{ABR})(1 - H(\phi_1))(1 - H(\phi_2))}{\sigma_{NR}\tau_1 + \sigma_{PAR}(\tau_2 - 2\tau_1) + \sigma_{ABR}(1 - H(\phi_1))(1 - H(\phi_2))},$$

where $\tau_1 = H(\phi_1)H(\phi_2)$ and $\tau_2 = H(\phi_1) + H(\phi_2)$.

The uncertainty map provides a digitalized uncertainty measurement for further analysis based on the numerical solution of the level set segmentation.

3.3.2. Lesion coloring

Areas of lesion generally occur in those regions of high uncertainty in each segmented region. Therefore, we mark these areas with different levels of emphasis according to the uncertainty measurement and the region segmented.

Color emphasis scheme: Although the uncertainty map is an objective uncertainty measure, it fails to provide direct visual cues. In this paper, we propose a way to combine the uncertainty map with the color channels to give efficient and direct visual aids to the dentist. To achieve the visual assistance, the RGB channels of the image are used to couple the intensity values of the image with the degree of uncertainty at each pixel. For all regions, the G channel is used to represent the intensity value of each pixel of the original dental X-ray image. The

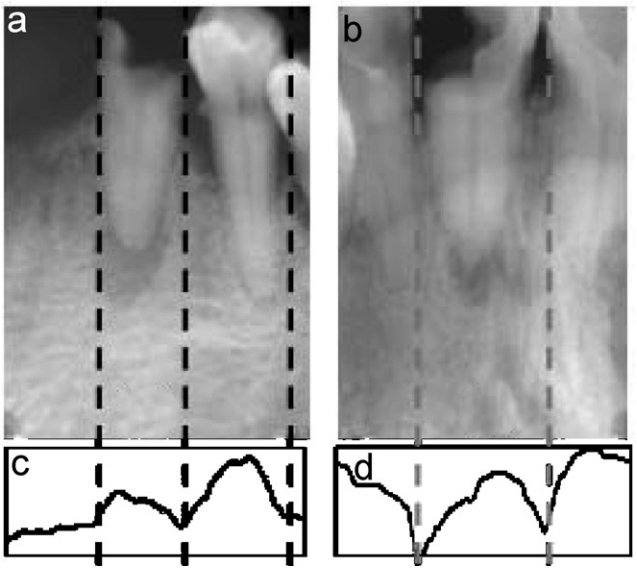

Fig. 8. Teeth isolation. (a) Original image 1. (b) Original image 2. (c) Integrated intensity profile of (a). (d) Integrated intensity profile of (b). The scales of the profiles in (c) and (d) are normalized to facilitiate comparison.

uncertainty values are nonlinearly scaled to the range 0–255. To differentiate between the three types of regions, for Ω_{ABR}, the R channel is set to the uncertainty value while the B channel is set to 0; for Ω_{PAR}, both the R and B channels are set to 255 to emphasize this region; and for Ω_{NR}, both the R and B channels are set to the uncertainty value.

3.3.3. Lesion detection

Lesion detection consists of three steps: tooth isolation, lesion location and seriousness level (SL) evaluation. This is a semi-automatic process in which the orientation of the teeth is supplied manually.

Teeth isolation: As suggested by Jain and Chen [1], individual teeth can be isolated by the integrated intensity value as shown in Fig. 8. The integrated intensity values sum the intensities of pixels along the vertical direction. Since the teeth usually yield higher intensity values than the jaws and other tissues, the gap of teeth will have a very low value on the integrated intensity value profile as shown in Fig. 8(c) and (d). However, unlike a dental forensic X-ray analysis, which can be assumed to have certain orientation, the clinical dental X-rays used to detect lesions, etc., could have any orientation. As shown in Fig. 9(a) and (c), if the orientation varies, this profile method will not be able to obtain the correct isolation. Therefore, as additional information, we assume that the orientation is given. Then we rotate the image according to the given orientation so that the teeth are aligned in a consistent direction. After the rotation, instead of using an integrated intensity value, we use the average of the intensity value (the integrated intensity value divided by the number of pixels) as shown in Fig. 9(b) and (d).

PL and BL location and SL evaluation: The PL and BL are detected with the following SL, in order of most serious to least serious: (1) SL: if the Ω_{ABR} is found at the area around root; (2) warning level (WL): if the Ω_{PAR} of any uncertainty is found; (3) attention level (AL): if a high uncertainty area of Ω_{NR} is found.

False positive (FP) removal: To improve the robustness and reduce the FP, the following three schemes are applied: (1) the SL of the lesions is decided by the most serious level; (2) the lesion region is assumed to be "round" shaped region. So the "nail like" shaped region will be ignored since they are usually either nerves or other noises; (3) the centerline projection curve or used to remove the FP caused by the nerves as shown in Fig. 10.

4. Experimental results

Altogether 60 dental X-rays with different level lesions are used to test the proposed framework and the results are validated by dentists. The promising results are demonstrated and analyzed in segmentation and analysis sections below separately.

4.1. Segmentation

First, images are used to test the proposed segmentation method. The results presented in Figs. 11–14, show that competitive level set segmentation is able to give pathologically meaningful segmentation. Areas of lesion are generally segmented as PAR, and the serious lesion are included in the abnormal and background region; the areas of early lesion are included in the NR. The pathologically meaningful segmentation is achieved by explicitly incorporating regions of problems as part of the modelling, such that those areas would be automatically segmented by the competition of the level set functions. Moreover, as shown in those figures, although the SVM only gives an approximate segmentation, it is able to provide good initial contours, closing to final segmentation results, for two level set functions, which not only accelerates the segmentation, but also provides competitive initial conditions for level set functions. Indeed, the competitive level set segmentation is robust to the placement of the initial contours so that even when the initial contours do not closely correspond to the final segmentation, the level set functions can still achieve an accurate segmentation as shown in Fig. 14, although with more iterations. Moreover, results show that our segmentation method is very robust to the large change of radiolucent in X-ray. Our segmentation method can successfully segment it into regions for further analysis even the quality is not good.

4.2. Analysis

The pathological segmentation provides a sound basis for analysis. Since the pathologically modelled competitive level set segmentation explicitly incorporates regions of problems as part of the modelling, the identification of lesion areas is an automatic product of the segmentation.

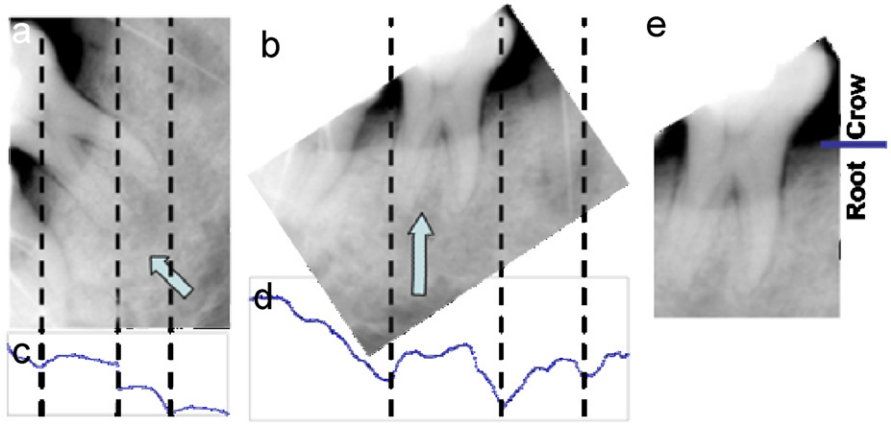

Fig. 9. Teeth isolation. (a) Original image. (b) Rotated image. (c) Integrated intensity profile of (a). (d) Average intensity profile of (b). (e) Two parts of a tooth: crown and root.

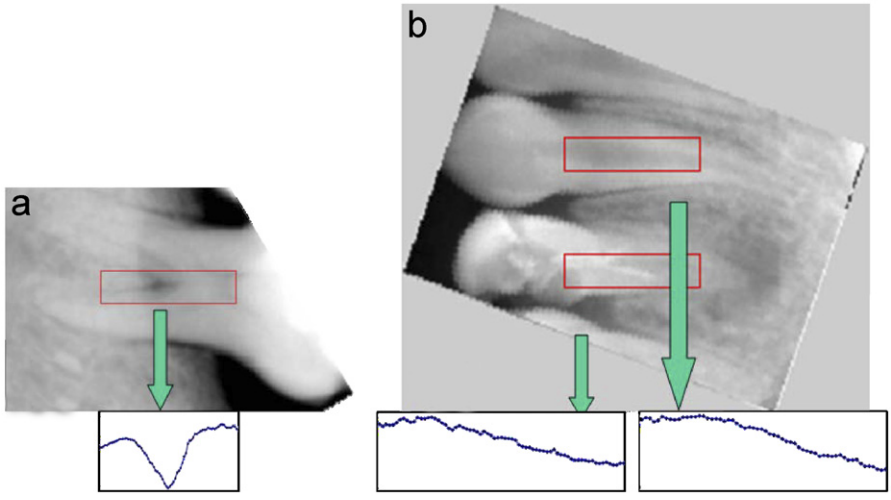

Fig. 10. Centerline projection curves. The curves are the vertical projections of the red marked areas in the images. (a) Projection curve of a area of lesion. (b) Projection curve of nerve.

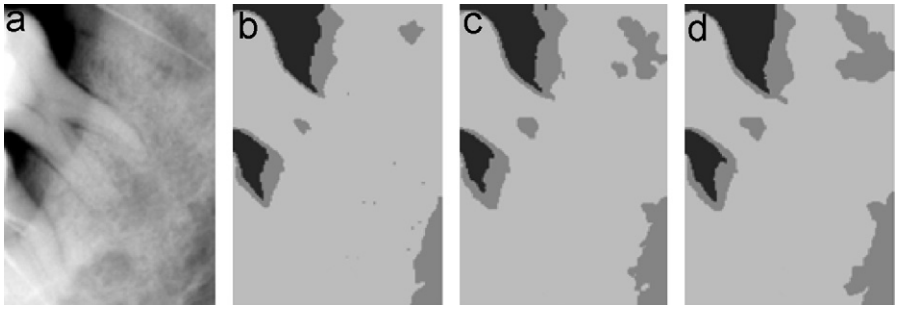

Fig. 11. Segmentation results. (a) Original image. (b) Iteration 0 provided by SVM. (c) Iteration 40. (d) Iteration 60.

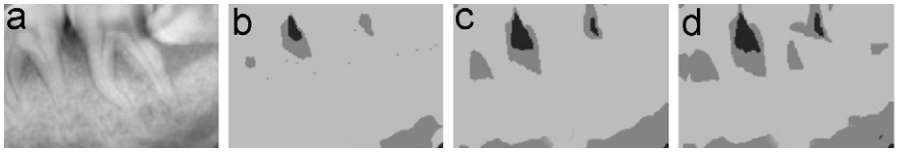

Fig. 12. Segmentation results. (a) Original image. (b) Iteration 0 provided by SVM. (c) Iteration 40. (d) Iteration 60.

Based on the uncertainty map and segmentation results, the color emphasis scheme is able to indicate all those radiolucent areas, which usually indicates areas of lesions when it is found in the area of bone, as shown in Figs. 15(b) and 16(b), in which those areas are lesions are emphasized by the color scheme. Since the soft tissue has the same intensity distribution, they are also marked.

The scheme provides direct visual cues, which will greatly reduce the possibility that some of these areas, the area indicated by an arrow in Fig. 15(b), for example, might be overlooked when their attentions are distracted by other areas or their main interest in the image. Although the area is segmented as a NR in the segmentation phase, the color channel scheme is able to highlight those areas for dentist's attention.

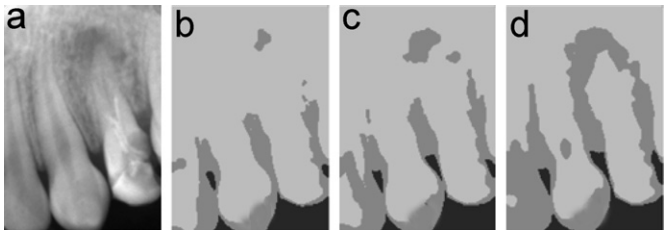

Fig. 13. Segmentation results. (a) Original image with lesion identified by dentist. (b) Initial condition provided by SVM. (c) Iteration 20. (d) Iteration 60.

Figs. 15–19 show the results of lesion detection. In the example shown in Fig. 15, after being given the orientation of the image, the color analysis scheme successfully locates the areas of lesions (see Fig. 15(c)). In this example, altogether the system automatically locates three lesions. Two of them are at the WL (pink area) and one is at the AL (orange area). In the example shown in Fig. 16, five areas of lesions are detected although one of them is FP. Fig. 17(d) shows a example where a FP is removed by the FP removal method. Fig. 18 shows another two examples on locating a WL area of lesion (pink area in Fig. 18(b)) and a serious level area of lesion (red area in Fig. 18(d)), although the quality of Fig. 18(c) is not very good. It is also interesting to observe that in Fig. 18(b), PAR around the first right tooth indicates the periodontic lesion beside the PL detected.

In the clinical practice, it is often the case that dentists are distracted by some factors such as the main interests or main answers they are looking for. And therefore, some less obvious lesions might be overlooked. With the assistance of our proposed method, the possibility of overlooking those areas are much reduced even when some distraction factors are present. In Fig. 15, the distraction might come from the root cannel treatment; in Fig. 16, the distraction might come from the caries, which is the main reason for that patient to take the X-ray; in Fig. 19, the distraction might come from the PL, while the periodontic lesion might be overlooked. Fig. 19 shows an example of locating a WL area of lesion (pink area in the figure).

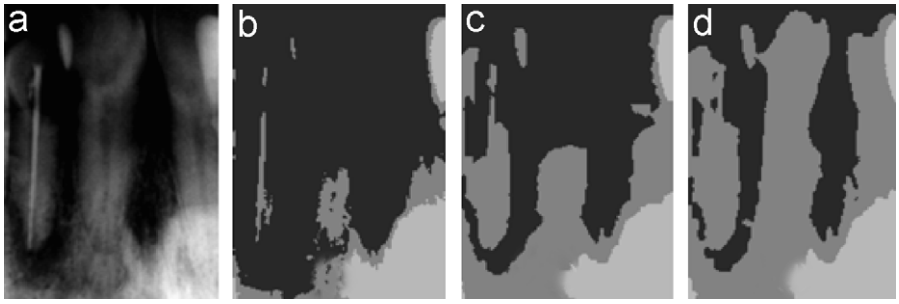

Fig. 14. Segmentation results. (a) Original image. (b) Iteration 0 provided by SVM. (c) Iteration 40. (d) Iteration 80.

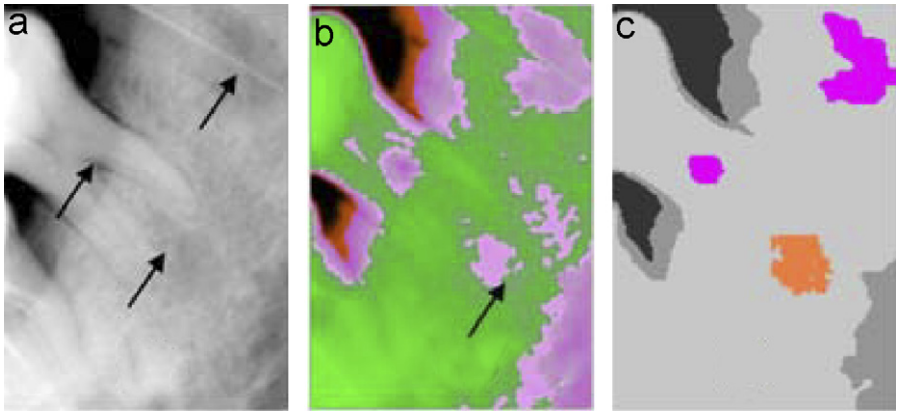

Fig. 15. Segmentation and lesion detection results. (a) Original image. (b) Areas of lesions marked with color channel method. (c) Areas of lesions detected.

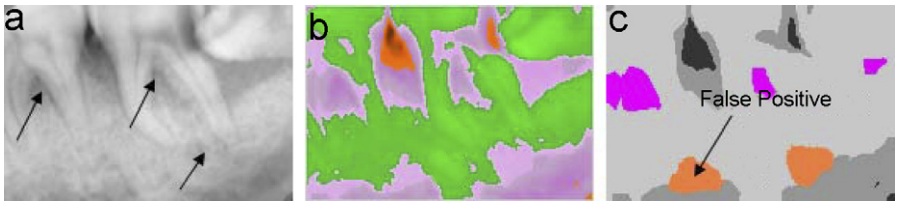

Fig. 16. Segmentation and lesion detection results. (a) Original image. (b) Areas of lesions marked with color channel method. (c) Areas of lesions detected.

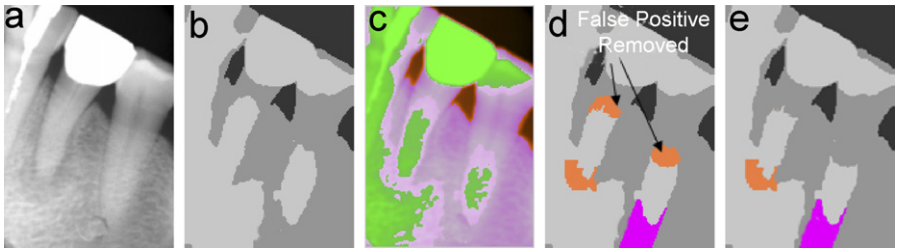

Fig. 17. Segmentation and lesion detection results. (a) Original image. (b) Segmentation result. (c) Areas of lesions marked with color channel method. (d) False positive removed by FP removal scheme. (e) Areas of lesions detected.

Fig. 18. Lesion detection results. (a),(c) Original image with lesion pointed by dentist. (b),(d) Areas of lesions detected.

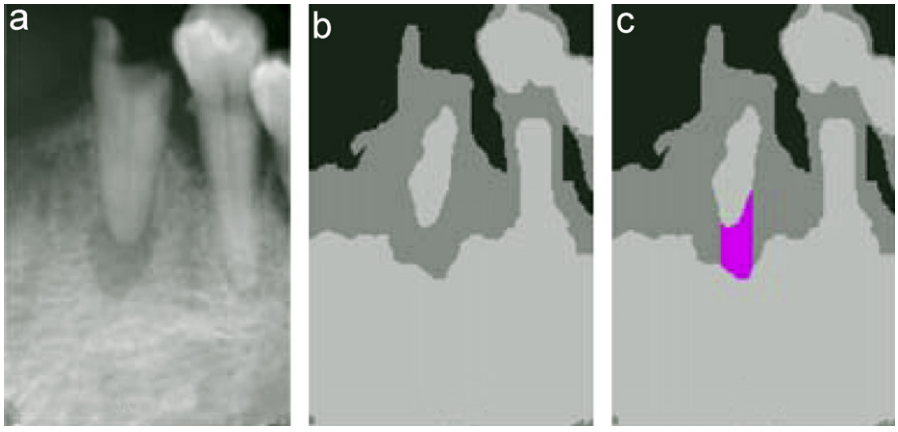

Fig. 19. Lesion detection results. (a) Original image. (b) Segmentation results. (c) Areas of lesions detected.

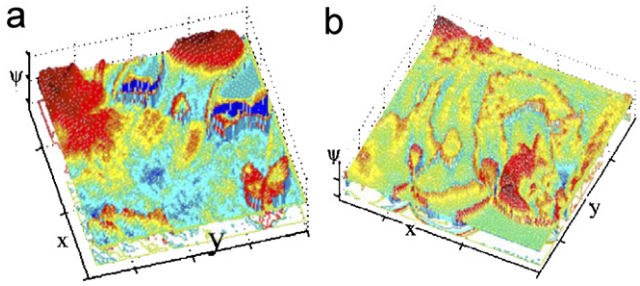

Fig. 20. Uncertainty maps of (a) Fig. 11 and (b) Fig. 13.

Fig. 20 shows two of visualized uncertainty maps. The uncertainty map is able to give a general idea of the problem areas. And more importantly, it provides a digitized uncertainty measurement for further analysis. The experimental results validated by dentists show that the proposed framework is able to help to find all the areas of lesions. For the lesion detection, the proposed framework is able to semi-automatically find all areas of lesion. But due to complexity of the dental X-rays, there are still nine FPs of lesion out of 181 lesion detected. One of these FPs is indicated by an arrow in Fig. 16(c).

5. Conclusions

Leveraging the transition towards a totally electronic format for dental X-rays, a framework to semi-automatically detect areas of lesion for computer aided dental X-rays analysis is proposed. The framework is designed, in particular, for the dental clinical setting through the use of a SVM and level set to ensure a fast and robust segmentation of these images. Utilizing these segmentations and a computed uncertainty map, regions of pathological abnormality are emphasized for the dentist's attention and two particular lesions can be automatically located, once the orientation of the teeth is given. Experimental results indicate that the system correctly identifies such problem areas with few FPs. The framework has the potential to be used in a dental clinical setting since the classifiers can be trained in advance and only the orientation of the X-ray image need be given or predetermined by the dentist.

References

[1] A.K. Jain, H. Chen, Matching of dental X-ray images for human identification, Pattern Recognition 37 (7) (2004) 1519–1532.
[2] H. Chen, A.K. Jain, Tooth contour extraction for matching dental radiographs, in: Proceedings of International Conference on Pattern Recognition, vol. III, Cambridge, UK, August 2004, pp. 522–525.
[3] G. Fahmy, D. Nassar, E. Haj-Said, H. Chen, O. Nomir, J. Zhou, R. Howell, H.H. Ammar, M. Abdel-Mottaleb, A.K. Jain, Towards an automated dental identification system (ADIS), in: International Conference on Biometric Authentication, vol. III, Hong Kong, July 2004, pp. 522–525.
[4] H. Chen, A.K. Jain, Dental biometrics: alignment and matching of dental radiographs, IEEE Trans. Pattern Anal. Mach. Intell. 27 (8) (2005) 1319–1326.
[5] S. Osher, J.A. Sethian, Fronts propagating with curvature-dependent speed: algorithms based on Hamilton–Jacobi formulations, J. Comput. Phys. 79 (1988) 12–49.
[6] S. Li, T. Fevens, A. Krzyżak, S. Li, Level set segmentation for computer aided dental X-ray analysis, in: Proceedings of SPIE Conference on Medical Imaging, vol. 5747, San Diego, USA, 2005, pp. 580–589.
[7] S. Li, T. Fevens, A. Krzyżak, S. Li, An automatic variational segmentation for dental X-ray analysis in clinical environment, Comput. Med. Imaging Graphics 30 (2006) 65–74.
[8] J. Deng, H.T. Tsui, A fast level set method for segmentation of low contrast noisy biomedical images, Pattern Recognition Lett. 23 (2002) 161–169.
[9] B. Nilsson, A. Heyden, A fast algorithm for level set-like active contours, Pattern Recognition Lett. 24 (2002) 1331–1337.
[10] M. Jeon, M. Alexander, W. Pedrycz, N. Pizzi, Unsupervised hierarchical image segmentation with level set and additive operator splitting, Pattern Recognition Lett. 26 (2005) 1461–1469.
[11] S. Osher, R. Fedkiw, Level set methods: an overview and some recent results, J. Comput. Phys. 169 (2001) 463–502.
[12] J. Sethian, Evolution, implementation, and application of level set and fast marching methods for advancing fronts, J. Comput. Phys. 169 (2001) 503–555.
[13] Y. Tsai, S. Osher, Level set methods in image science, in: International Conference on Image Processing, vol. 169, Barcelona, Spain, 2003, pp. 631–634.
[14] H.-K. Zhao, T.F. Chan, B. Merriman, S. Osher, A variational level set approach to multiphase motion, J. Comput. Phys. 127 (1) (1996) 179–195.
[15] T. Chan, L. Vese, Active contour without edges, IEEE Trans. Image Process. 24 (2001) 266–277.
[16] M. Holtzman-Gazit, D. Goldsher, R. Kimmel, Hierarchical segmentation of thin structure in volumetric medical images, in: Medical Image Computing and Computer-Assisted Intervention (MICCAI), Montreal, 2003.
[17] A. Tsai, A. Yezzi, A.S. Willsky, Curve evolution implementation of the Mumford–Shah functional for image segmentation, denoising, interpolation, and magnification, IEEE Trans. Image Process. 10 (2001) 1169–1186.
[18] L. Vese, T. Chan, A multiphase level set framework for image segmentation using the Mumford and Shah model, Int. J. Comput. Vision. 50 (3) (2002) 271–293.
[19] C. Samson, L. Blanc-Fraud, G. Aubert, J. Zerubia, A level set model for image classification, Int. J. Comput. Vision 40 (3) (2000) 187–197.
[20] R. Kimmel, A.M. Bruckstein, Regularized Laplacian zero crossings as optimal edge integrators, Int. J. Comput. Vision 53 (2003) 225–243.
[21] S. Li, T. Fevens, A. Krzyżak, A SVM-based framework for autonomous volumetric medical image segmentation using hierarchical and coupled level sets, in: CARS, International Congress Series, vol. 1268, Chicago, USA, Elsevier, Amsterdam, 2004, pp. 207–212.
[22] S. Li, T. Fevens, A. Krzyżak, Image segmentation adapted for clinical settings by combining pattern classification and level sets, in: Medical Image Computing and Computer-Assisted Intervention (MICCAI),

St-Malo, France, Lecture Notes in Computer Science, vol. 3216, Springer, Berlin, 2004, pp. 160–167.

[23] A. Tsai, J. Yezzi, A. Willsky, Curve evolution implementation of the Mumford–Shah functional for image segmentation, denoising, interpolation, and magnification, IEEE Trans. Image Process. 10 (2001) 1169–1186.

[24] S. Li, T. Fevens, A. Krzyzak, S. Li, Automatic clinical image segmentation using pathological modelling, PCA and SVM, in: P. Perner A. Imiya, (Eds.), Machine Learning and Data Mining in Pattern Recognition, Lecture Notes in Artificial Intelligence, vol. 3587 (Leipzig, Germany), Springer, Berlin, 2005, pp. 314–324.

[25] V. Caselles, R. Kimmel, G. Sapiro, Geodesic active contours, Int. J. Comput. Vision 22 (1997) 61–79.

[26] C.-C. Chang, C.-J. Lin, Training nu-support vector classifiers: theory and algorithms, Neural Comput. 13 (9) (2001) 2119–2147.

[27] M. Turk, A. Pentland, Face recognition using eigenfaces, in: Proceedings of IEEE Conference on Computer Vision and Pattern Recognition, Hawaii, 1991.

[28] M. Turk, A. Pentland, Eigenfaces for recognition, J. Cognitive Neurosci. 3 (1) (1991) 71–86.

About the Author—SHUO LI obtained his Ph.D. degree from Concordia University, Canada on March 2006. He obtained his B.E. and M.E. degrees from China, in 1996 and 1999. He is working in GE Healthcare as a research scientist. He is also an adjunct research professor in University of Western Ontario. His current interest is in computer aided medical image analysis and visualization.